UserCom
2/2002

Information for users of METTLER TOLEDO thermal analysis systems

16

Dear Customer

The STAR^{e} system has once again found very many new users in 2002. The range of applications has now been greatly expanded thanks to the introduction of the exciting new DMA/SDTA861^{e} Dynamic Mechanical Analyzer and, more recently, the high pressure DSC827^{e} module. The STAR^{e} System is extremely versatile and is nowadays used in practically all industries for both quality assurance and research purposes.
In UserCom we often publish articles from somewhat less well-known application areas. We hope that these applications will encourage you to try out one or the other in you field of work.

Contents

Interpreting DMA curves, Part 2

Dr. Jürgen Schawe

Introduction

Part 1 of this series of articles (UserCom15) covers non-isothermal DMA measurements and the dependence of the mechanical modulus on temperature. This second article deals with the frequency dependence of the mechanical properties and quantities of stable samples. Because of the enormous scope of this field, only the basic principles and general rules that explain the behavior of materials are discussed.
In practice, materials are subjected to stresses at many different frequencies. It is therefore extremely important to have a detailed understanding of the effect of frequency on mechanical properties. In addition, it means that materials need to have different properties under different conditions. For example, an adhesive should behave elastically without breaking when it suffers a blow (high frequencies), but should at the same time be able to "accommodate" stress arising from temperature fluctuations (low frequencies) like a liquid.

Complex modulus and compliance

An ideal elastic solid

In shear mode, DMA measures the shear modulus, G*, and the shear compliance, J*. An ideal elastic material stores the entire mechanical energy responsible for the deformation. When the shear stress is removed, this energy is liberated. The modulus is independent of frequency; stress and deformation (strain) are in phase. In this situation, $G^* = G'$, whereby G' is known as the storage modulus. An example that illustrates this behavior is that of a spring (Fig. 1a).

An ideal viscous liquid

In an ideal liquid, the applied stress and the strain are phase-shifted by 90°. Because the molecules are free to move, no mechanical energy is stored in the material - the energy is completely converted to heat. The corresponding model is the damping device shown (Fig. 1b). Typically, a liquid is described with the frequency-independent viscosity η_0. In the case of the shear modulus, $G^*(\omega) = iG''(\omega)$. The imaginary number, $i = \sqrt{-1}$, is a mathematical expression that represents the fact that the mechanical energy is dissipated, i.e. converted to heat. G'' is the loss modulus, where $G'' = \omega\eta_0$. In a liquid, the loss modulus therefore increases linearly with the frequency, f, where $f = \omega/2\pi$.

Viscoelastic materials

In real materials, the reaction to an external stress is accompanied by molecular rearrangements that take place over a wide frequency range. Examples of this are lattice vibrations in solids at about 10^{14} Hz and cooperative rearrangements at the glass transition at about 10^{-2} Hz. Molecular rearrangements are the reason for the different relaxation processes. At higher temperatures, the frequency of the molecular rearrangements increases. The resulting temperature dependence of the relaxation process is discussed in another article in this publication (UserCom16, page 10). The properties of real materials lie between those of an ideal liquid and an ideal solid. Due to the fact that they have both elastic and viscous properties, the materials are said to be viscoelastic. Their behavior is described mathematically by the complex, frequency-dependent modulus

$$G^*(\omega) = G'(\omega) + iG''(\omega) \qquad (1)$$

where G' is the elastic part of the modulus and G'' the energy dissipation part (viscous component). Technical models that illustrate viscoelastic behavior are combinations of springs and damping devices (Fig. 1c).

The complex compliance

The G* modulus describes the relaxation of the mechanical stress for a given strain. In everyday language, a material with a larger storage modulus is said to be "harder".
The DMA experiment can also be performed in such a way that the stress is given and the resulting strain is measured. One then talks of strain retardation. The retardation time is a measure of the time delay in the strain after imposition of the stress. In this case, the compliance, J*, is determined. This is also complex and frequency dependent and is given by

$$J^*(\omega) = J'(\omega) - iJ''(\omega) \qquad (2)$$

where J' and J'' are the storage and loss compliances. In simple terms, one can say that a "softer" material has a greater (storage) compliance.
The relationship between modulus and compliance is given by the equation

$$J^*(\omega) = 1/G^*(\omega) \qquad (3)$$

This allows the following equations to be derived:
$J' = G'/(G'^2 + G''^2)$ and
$J'' = G''/(G'^2 + G''^2)$.
The relationship between the modulus, compliance and loss factor ($\tan\delta$) for a relaxation process is illustrated in Figure 2.

The mechanical behavior of a material can be expressed equally well using the modulus or the compliance. In practice, the quantity used depends on what you are accustomed to, or to practical considerations. For example, the modulus is often used when discussing mechanical behavior in the rubbery plateau, whereas the compliance is used to separate different processes.

The frequency dependence of modulus and compliance

An overview of frequency dependence

Figure 3 displays schematic curves of the moduli and compliances for an amorphous polymer. The curves are displayed in log-log presentation. At low frequencies one can see the flow region, in which G'

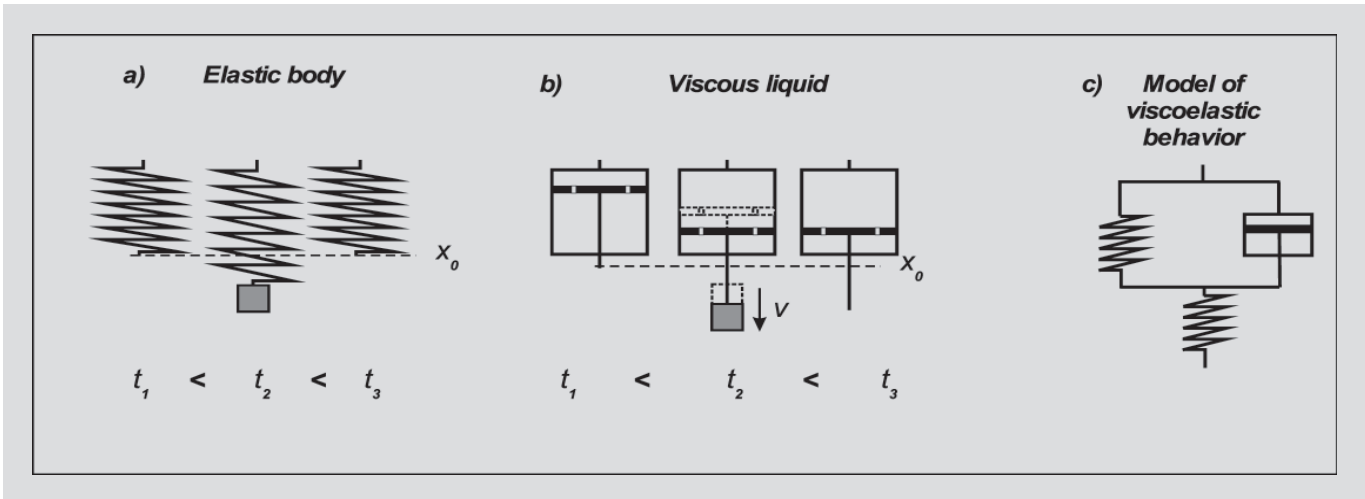

Fig. 1. Models illustrating the mechanical behavior of materials. t_1, t_2 and t_3 are the times before, during and after the load was applied, x_0 is the initial length and v is a constant rate.

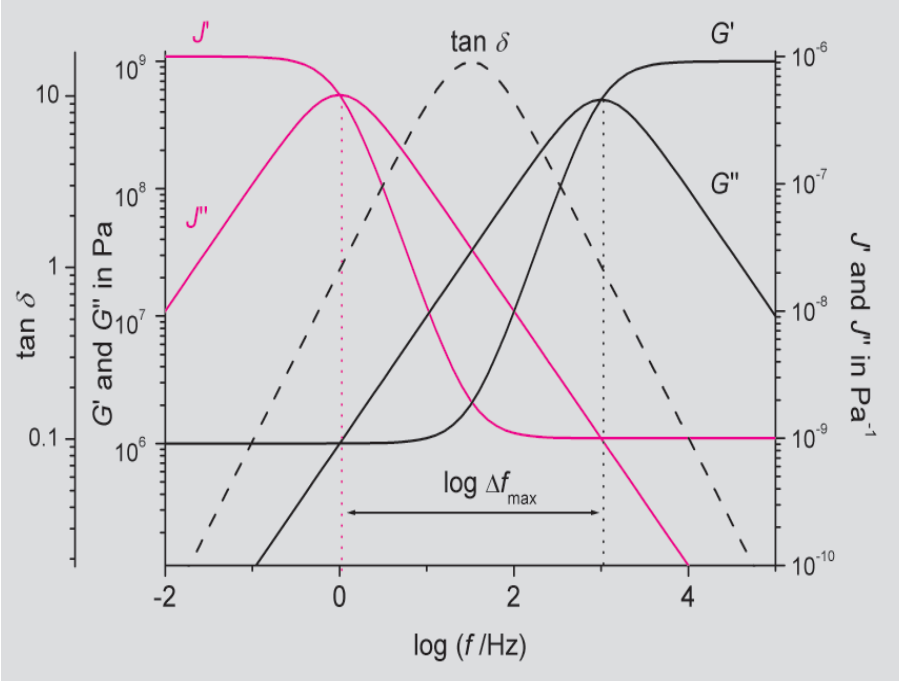

Fig. 2. Basic curve shapes of moduli, compliances and tan δ as a function of frequency.

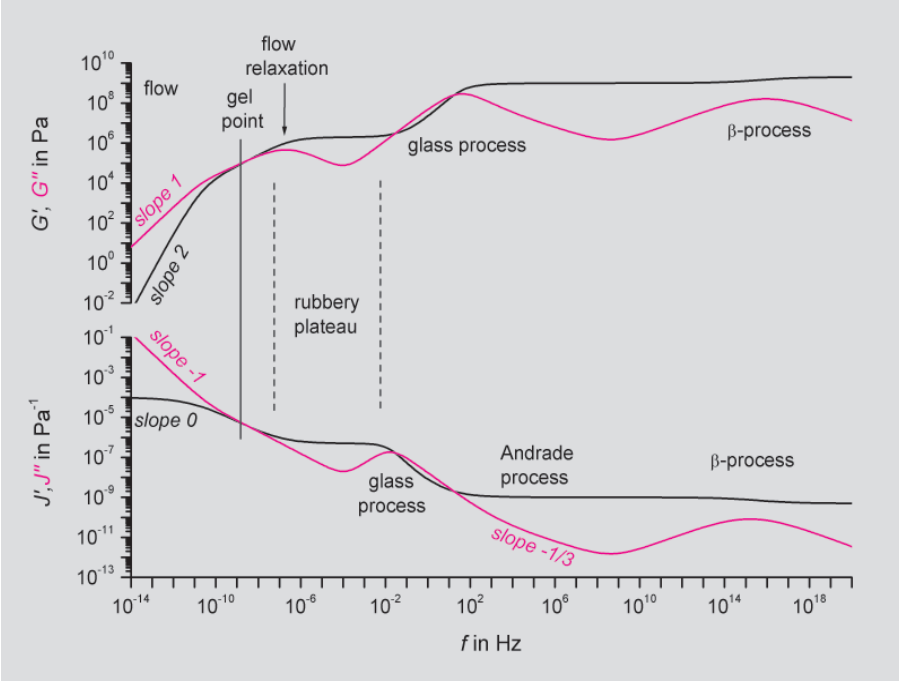

Fig. 3. Schematic curves of moduli and compliances for a viscoelastic material.

and G″ increase with frequency and J′ and J″ decrease. There then follows the region of flow relaxation and the rubbery plateau in which G′ and J′ are almost constant. A large step in the storage part is characteristic for the main relaxation region. In the transition region, the loss components exhibit peaks. At higher frequencies, secondary relaxation (β-relaxation) occurs. The resulting steps in G′ and J′ and peaks in G″ and J″ are then relatively broad. A number of different relaxation processes occur over the entire frequency range. The frequency corresponds to the characteristic length of the molecular rearrangement considered. The greater the frequency, the smaller is the characteristic length. With secondary relaxation, the characteristic length is about 0.5 nm, whereas at the main relaxation (maximum of G″) it is about 2.5 nm and at the corresponding maximum of J″ about 5 nm.

The β-relaxation observed in polymers is often attributed to the side chains. With polymers that do not have movable side chains, it is interpreted as a conformational variation or fluctuation. The nature of these relaxation effects cannot however be reduced to polymer specific processes because it is also observed in low molecular weight glass formers.

Figure 4 displays the modulus of unvulcanized styrene-butadiene rubber (SBR) at -10 °C. The individual effects are discussed in the following sections.

Behavior in the glassy state

We begin the discussion of the mechanical behavior at high frequencies. In Figure 4, the storage modulus, G′, is almost constant above 10^5 Hz and the loss modulus is orders of magnitude (decades) less than G′. The frequency of the mechanical stress fluctuation is much greater than the characteristic frequency of the liquid-specific cooperative rearrangements. This means that these molecular processes, which are the origin of the liquid properties, are not activated. The material behaves just like an elastic solid. As shown in Figure 3, secondary or β-relaxation occurs. With SBR, this process lies outside the actual range measured. At frequencies below the β-relaxation, the Andrade process is often observed. Here the frequency dependence of J″ is described by an exponential law, namely $J'' \propto \omega^{-1/3}$. The loss compliance has a slope of -1/3 in the log-log presentation. With SBR, this region can be seen between 10^5 and 10^8 Hz (see Fig. 5).

The glass process

The relaxation region in which the storage modulus changes by several orders of magnitude is the glass transition (the main relaxation or α-relaxation). This relaxation process is measured when the measuring frequency lies in the frequency range of the cooperative rearrangements. If the frequency is lowered still further, the material loses its solid-state properties. With SBR (Fig. 4), G′ changes from about 10^9 Pa to 10^6 Pa with decreasing frequency. The maximum of the corresponding G″ peak is at a frequency of $3 \cdot 10^2$ Hz at -10 °C. The compliance shows analogous behavior except that J′ increases with decreasing frequency (Fig. 5). The maximum of the J″ peak is at 10^{-1} Hz (Fig. 5). Characteristic

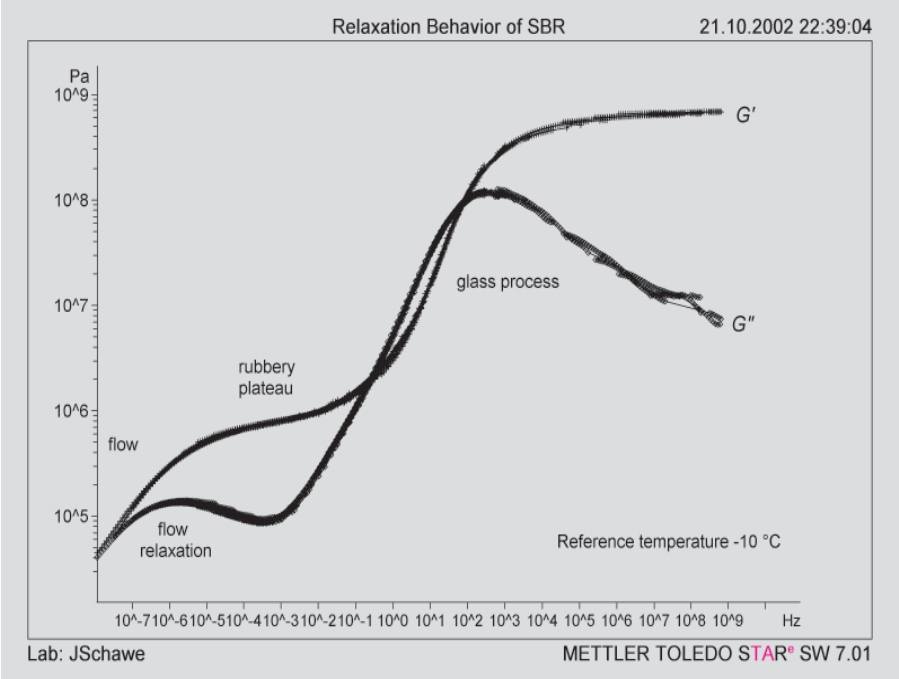

Fig. 4. Storage and loss modulus of SBR at -10 °C.

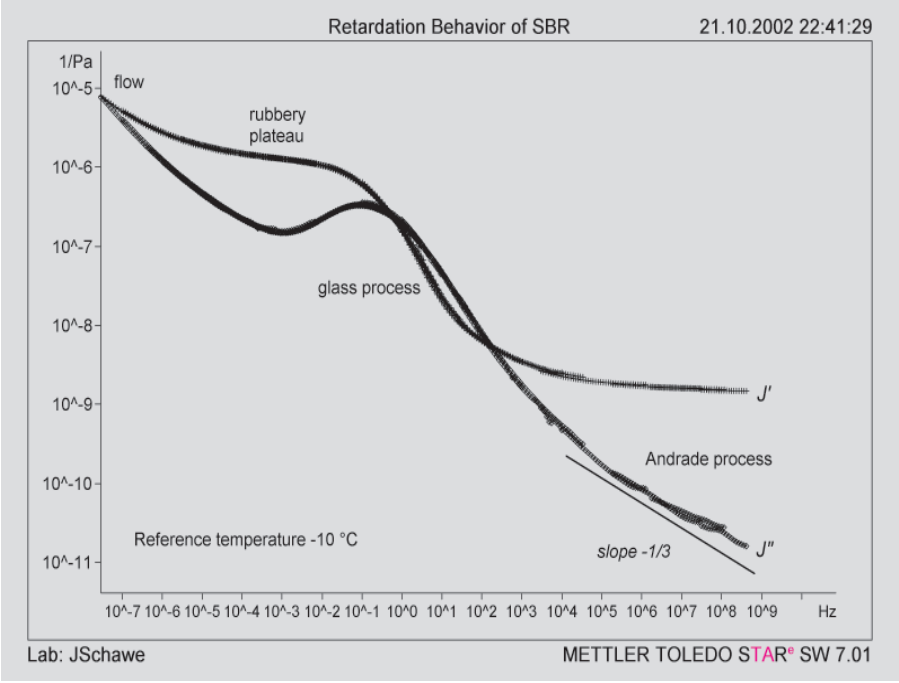

Fig. 5. Storage and loss compliance of SBR at -10 °C.

quantities of the cooperative rearrangements are the relaxation time, τ_G, and the retardation time, τ_J. At the maximum of the loss peak $\omega \cdot \tau \approx 1$. The retardation time of SBR at -10 °C is therefore given by the equation $\tau_J = 1/(2\pi \cdot 10^{-1})$ s, i.e. 1.6 s. Since the relaxation region is measured at higher frequencies in the modulus, the relaxation time, τ_G, is $5.3 \cdot 10^{-4}$ s.

If one considers the simplest possible process for retardation, namely the Debye process (which describes a retardation process with just one single retardation time), then the following equation applies

$$J^*(\omega) = J_0 + \frac{J_\infty - J_0}{1 + i\omega\tau_J} \qquad (4)$$

Here J_0 and J_∞ are the limiting values of the compliance at low and high frequencies. The relationship between the retardation and relaxation time is then given by the equations $\tau_G = \tau_J (\log J_0 - \log J_\infty)$ and $\tau_J = \tau_G (\log G_\infty - \log G_0)$. The logarithmic distance, log Δf, between the maxima of the J″ and G″ peaks can then be estimated to be 3.0 (see Fig. 2). The experimental result (3.5) shows that this simple estimate is also approximately valid for real processes. The relatively large distance between the J″ and G″ peaks therefore results from the large change in G′ and J′ at the glass transition.

The shape of the transition provides further information on the relaxation behavior. The curve shape of an isolated process is shown in Figure 6 using J″ as an example. In the log-log presentation, the Debye process has two linear limiting tangents with slopes of 1 and -1. The width at half height of the peak is 1.14 frequency decades. Real processes show appreciably broader peaks - due to molecular interaction there is not just one retardation time but a wide spectrum of times. This results in a broader J″ peak with the slopes of α and $-\alpha\gamma$, where $0 < \alpha \leq 1$ and $0 < \alpha\gamma \leq 1$. The quantities α and γ are known as Havriliak-Negami (HN) prameters and describe the width of the relaxation transition.

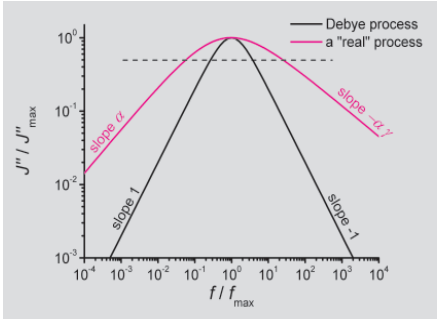

Fig. 6. Curve shape of the loss compliance in the retardation region in log-log presentation. The dashed line marks half the peak height.

The location and width of the relaxation transitions are very sensitive to changes in physical and chemical structure (e.g. to crystallization and changes in the polymer chain), and to fillers, plasticizers and composition in the case of polymer blends or copolymers. Some examples are illustrated in Figure 7.

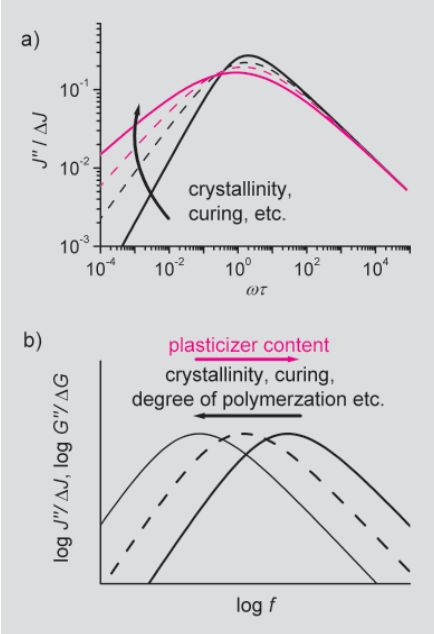

Fig. 7. Schematic curves of different factors that influence the glass process: a) influence of curve shape; b) shift of the frequency position (the arrow indicates the direction of increase of the corresponding quantity).

The rubbery plateau

Low molecular weight substances begin to flow on decreasing the frequency immediately after the glass transition. Polymers have a characteristic modulus, G_0, of about 1 Mpa in the rubbery plateau. The plateau is due to the entanglement of macromolecules to form a physical network. The width of the plateau, log Δf, depends on the molecular weight, M, where $\log \Delta f \propto M^{3.4}$ (Fig. 8). In the plateau, G″ is less than G′. In the middle of the plateau, G″ has a minimum (Fig. 4). At the end of the plateau, flow relaxation can be seen on the G″ peak (with SBR in Fig. 4 at 10^{-6} Hz). This process cannot usually be seen directly in the compliance curve because it is overlaid by flow.

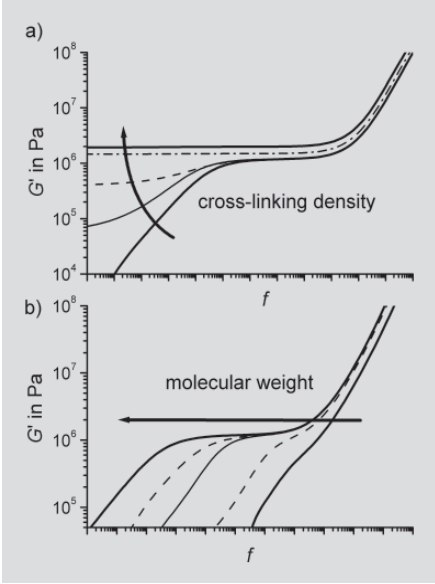

Fig. 8. Schematic curves showing the influence of the degree of cross-linking (a), and molecular weight (b) on the rubbery plateau (the arrow indicates the direction of increase of the corresponding quantity).

With cross-linked materials such as vulcanized elastomers, the plateau modulus, G_0, is proportional to the mean cross-linking density, κ, where $\kappa \approx G_0/(2RT)$. Flow relaxation can only be observed with very lightly cross-linked materials (Fig. 8).

Viscous flow

At very low frequencies, uncross-linked polymers flow. In the ideal case, the power laws $G' \propto \omega^2$ and $G'' \propto \omega$ apply. Here the slopes of the modulus curves in log-log presentation are 2 for G′ and 1 for G″. At the gel point, the G′ and G″ curves cross over one another.

Conclusions

Knowledge of the frequency dependence of mechanical behavior is of great value for the practical application of materials and for material optimization. Information is obtained for material optimization because the frequencies at which the different processes occur correlate with the characteristic volumes of the corresponding molecular regions. At higher frequencies, smaller molecular regions are observed.
In comparison to temperature-dependent measurements, frequency-dependent measurements provide additional information about material properties in general and on molecular processes in particular.

New in our sales program

HP DSC827^e

The new high pressure DSC module replaces the TC15/DSC27 combination. The following points have been improved in the new pressure cell:

- The maximum pressure now available is 10 MPa (100 bar)
- The cooling rate has been greatly increased through an additional jacket cooling system.
- The latest DSC furnace technology has been used
- New FRS5 sensor similar to that in the DSC822^e

The same gas supply system and pressure vessel as before are used. STAR^e SW Version ≥ V7.xx is needed to control the HP DSC827^e.
The new HP DSC827^e module offers excellent performance.

Specifications

Pressure range (overpressure)	0 to 10 MPa
Temperature range	22 - 600 °C
Temperature accuracy	+/- 0.2 °C
Temperature reproducibility	+/- 0.1 °C
Sensor type	FRS5 ceramic sensor with 56 Au/AuPd thermopile
Signal time constant	2.3 s
Measuring range	700 mW
Digital resolution	16 million points
Sampling rate	Max. 10 points per second (selectable)

Application possibilities

We foresee the following application possibilities for the high pressure DSC:

Industry	Applications
Chemical and pharmaceutical industries and universities	- Reactions with reactive gases (e.g. O_2, H_2, CO_2) - Reactions in pure, poisonous or fuel atmospheres - Safety investigations - Suppression of vaporization (through increase of the boiling point) - Separation of chemical reactions and vaporization that overlap at normal pressure - Investigation of reactions with volatile components - Catalytic reactions - Heterogeneous reactions - Adsorption and desorption - Measurement of the pressure dependence of the boiling point - Determination of enthalpy of vaporization
Petrochemical	- Oxidation stability (e.g. checking of oil additives in lubricants) - Reactions with reactive gases
Plastics	- Curing of polymers (e.g. polycondensations) - Oxidation stability
Paints/lacquers/adhesives	- Cross-linking of adhesives - Suppression of vaporization (through increase of the boiling point)
Electronics industry	- Curing of resins (e.g. polycondensation)
Foodstuffs	- Oxidation stability of fats and oils - Reactions with reactive gases

Application example

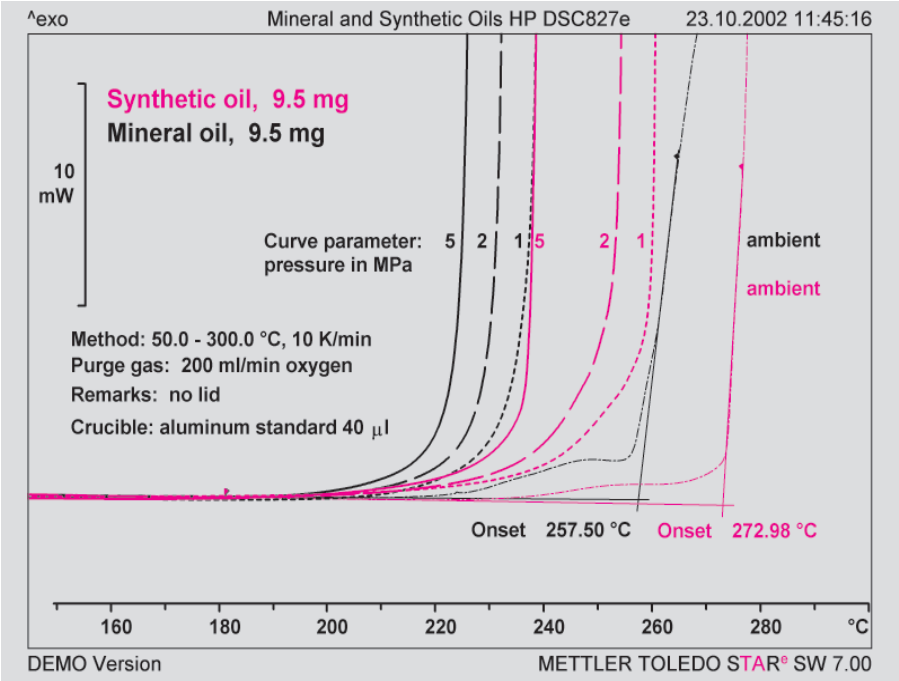

Fig. 1. Comparison of the oxidation of a regular mineral oil with that of a synthetic oil at various oxygen pressures. The mineral oil oxidizes at significantly lower temperatures than the synthetic oil at the same oxygen pressure. In this example, the HP DSC827e module allows the lubricant oil to be analyzed under realistic conditions, i.e. such as occur at the operating temperature in an engine between the bearings and the crankshaft.

DSC and TGA crucible sets

These two crucibles sets allow you to perform measurements with different crucibles but without the need for you to purchase a complete set of every type of crucible. Both sets also contain the corresponding lids.

Choosing the right crucible is of utmost importance in thermal analysis. The crucible influences the

- quality of the measurement and
- the performance of the instrument.

- Low mass crucibles allow better separation of overlapping effects
  ➔ shorter signal time constants lead to better temperature resolution
- Crucibles with low wall heights facilitate fast decomposition reactions
  ➔ better gas exchange between sample and atmosphere
- Crucibles with lids, or lids with a hole of µm-size retard vaporization
  ➔ better separation of overlapping effects
- The crucible material also influences the measurement. A catalytic effect (e.g. platinum crucible) may, or may not be desirable
  ➔ samples are influenced, or not influenced by the crucible material
- Large volume crucibles allow larger sample amounts to be measured
  ➔ the sensitivity can be improved

DSC crucible set (ME 51 141 278)

Crucible type	Volume (µl)	Pieces
Aluminum standard	40	10
Aluminum light	20	10
Crucible lid (with 50-µm hole)	-	20
Gold	40	2
Aluminum	100	10

TGA crucible set (ME 51 141 279)

Crucible type	Volume (µl)	Pieces
Aluminum standard	40	10
Platinum	30	1
Sapphire	70	1
Alumina	30	2
Aluminum	100	10

Characterization of drugs by DSC

Camelia Nicolescu; Corina Arama (with the support of Prof. Dr. Pharm. Crina Maria Monciu) Department of Analytical Chemistry, "Carol Davila" School of Pharmacy, Traian Vuia Str. No.6, 70139 Bucharest, Rumania

Introduction

It is well known that interactions between the active substance and excipients can influence the pharmacological properties and behavior of drugs in biological systems.

In this study, mixtures of excipients and piroxicam as the active substance were ground together and analyzed by DSC.

The active substance, piroxicam (4-hydroxy-2-methyl-N-pyridinyl-2H-1,2-benzothiazine-3-carboxamide 1,1-dioxide) is a non-steroidal drug that is often used for the treatment of osteoarthritis and rheumatoid arthritis. It shows a therapeutic effect in very small doses and has few side effects. The drug's mechanism has to do with the disruption of prostaglandin formation and inhibition of the enzyme cyclooxygenase.

Besides the active substance itself, piroxicam tablets contain the following excipients: anhydrous lactose, lactose monohydrate, microcrystalline cellulose type 102 and magnesium stearate.

Experimental details

Measuring cell:	DSC821^e,
Crucible:	aluminum 40 µl, lid with 50-µm hole to produce a self generated atmosphere
DSC program:	heating from 75 to 200 °C at 2 K/min
Atmosphere:	stationary air

Measurements and results

The mixture of excipients and the active substance were first measured separately. The excipients curve shows a melting peak at 140 °C, while the active substance (piroxicam) melts at 202 °C (Fig. 1).

A series of mixtures was then prepared by finely grinding the mixture of excipients with increasing amounts of piroxicam. Figure 2 displays the DSC curves of some of these samples.

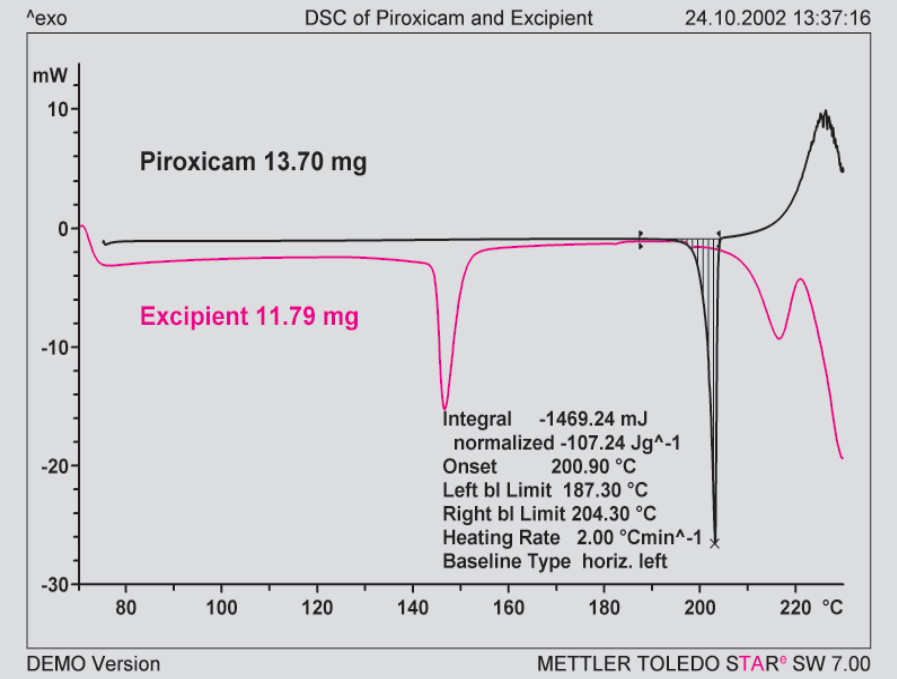

Fig. 1. DSC curves of pure piroxicam and the mixture of excipients (anhydrous lactose, lactose monohydrate, microcrystalline cellulose type 102 and magnesium stearate). Heating rate 2 K/min. The pure piroxicam exhibits a sharp melting peak that appears well separated from the decomposition peak that follows. The excipients curve shows three effects: drying at 100 °C; melting/loss of water of crystallization of the lactose from 110 to 150 °C; decomposition of the lactose from 190 °C onward.

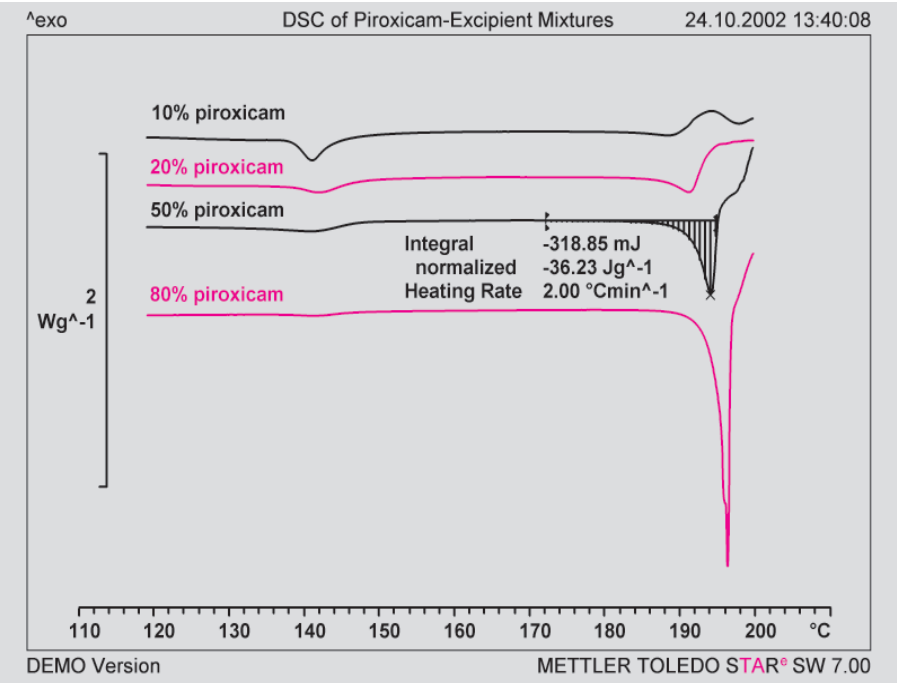

Fig. 2. DSC curves of mixtures with different contents of piroxicam; heating rate 2 K/min, sample weight 8 to 12 mg. Reactions of individual excipients occur below 160 °C. The piroxicam melting peak appears in the range 185 to 200 °C and is followed by immediate exothermic decomposition. The baseline type "horizontal from left" was therefore chosen to calculate the peak area (see example with 50% piroxicam).

The mixtures show an endothermic effect just below 200 °C. This is attributed to the melting of the active substance. The fact that the melting temperature is lower (up to 10 K) can only be explained by assuming that there is a non-eutectic interaction between the substance and the excipients. The nonlinear increase in surface area is also evidence supporting an interaction (Fig. 3).

The DSC curve of the piroxicam tablet (200 mg, manufactured by Terapia, Cluj, Rumania) is similar to that of the sample with the same piroxicam content prepared by grinding piroxicam with the excipients (Fig. 4).

Conclusions

The DSC curves show that interactions occur between the different constituents, both in the samples obtained by grinding the active substance with the excipients and in the piroxicam tablet itself. The interactions become less and less important with piroxicam contents greater than 60%. Once the nonlinear relationship between the enthalpy of melting and the content of the active substance has been established, the DSC piroxicam peak area can be used to calculate the content of the active substance for quality control purposes.

Literature

[1] *Thermal Analysis of a drug-polymeric excipient solid system*
F.Giordano, G.P. Bettinetti, A. La Manna, A. Marini, V. Berbenni
J. Thermal Anal. 34, 1988

[2] *Effect of compressional forces on piroxicam polymorphs*
G.A. Ghan, J.K. Lalla
J. Pharm.Pharmacol. 1992, 44

[3] *Bazele farmacologice ale practicii medicale*
V. Stroescu
Ed. Medicala, ed. VII, 2001

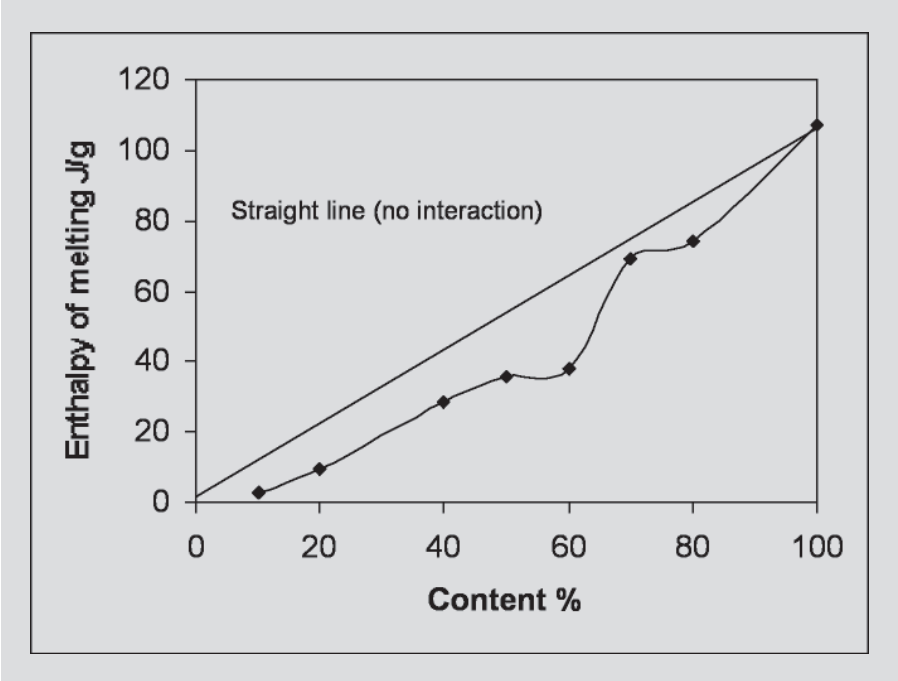

Fig. 3. Up until a piroxicam content of 60%, the enthalpy of melting of samples with increasing piroxicam content remains appreciably less than that expected from the straight line drawn for no interaction.

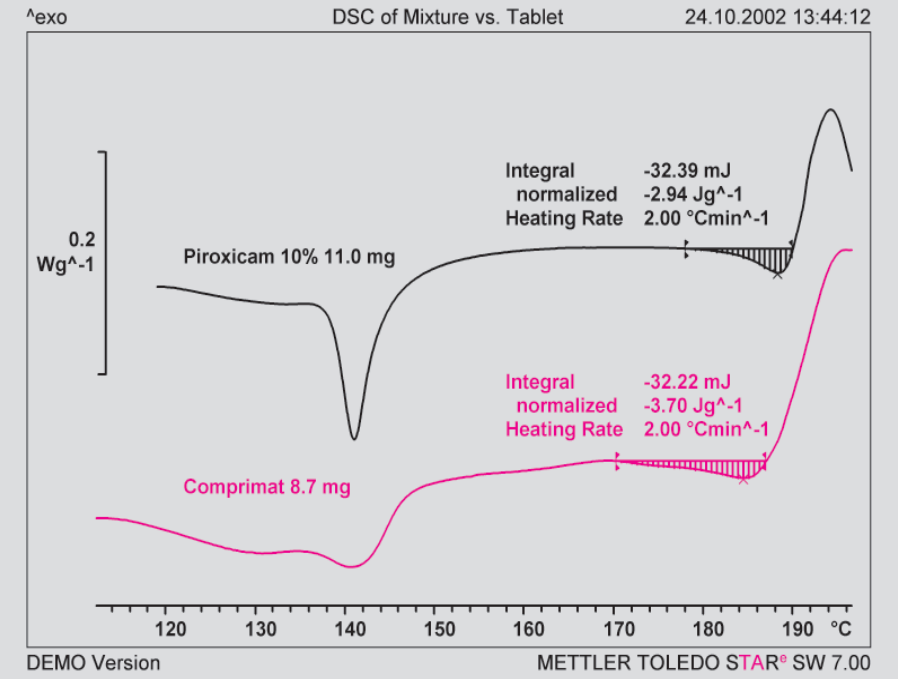

Fig. 4. Below 160 °C, in the region of the excipients peak (moisture, water of crystallization), the DSC curve of the tablet (Comprimat 8.7 mg) is somewhat different to the curve of the sample with the same piroxicam content (10%) obtained by grinding piroxicam with the excipients. The curves are, however, very similar in the region in which the piroxicam melts.

Determination of the glass temperature by dynamic mechanical analysis

Dr. Claus Wrana, Bayer, Leverkusen, Germany

Introduction

The glass transition temperature is a important criterion for the technological use of polymeric materials. The application range of elastomers is usually restricted to temperatures significantly above the glass transition temperature to ensure that deformation behavior is as far as possible entropy elastic.

The glass transition temperature of a polymer is, however, strongly dependent on frequency, and the deformation of elastomers is usually time dependent (e.g. seals, surface of tires, etc.). This means that a glass transition temperature measured under quasi static conditions (for example by DSC) is not a good criterion for the characterization of the low temperature behavior of dynamically stressed materials.

The temperature limits for dynamically stressed elastomeric materials can be determined by measuring the glass transition temperature using methods in which a periodic stress is applied. The measurement frequency should of course correspond to the frequency at which the component is in practice stressed.

If such a measurement is not possible, for example at frequencies that are significantly higher or lower than the measurement range of the instrument, then the glass transition temperature can be obtained by extrapolation using the time-temperature superposition principle. A quantitative relationship between the glass transition temperature and measuring frequency can be obtained through the semi-empirical WLF or analogous Vogel-Fulcher equation.

In this article, the experimental relationship between frequency and time are determined for a number of primary elastomers (NR, BR, SBR, NBR, IIR) from temperature-dependent and frequency-dependent shear modulus measurements. The quantitative description of the time-temperature superposition principle is performed using the semi-empirical WLF or analogous Vogel-Fulcher equation.

Samples and sample preparation

Samples for frequency and temperature-dependent measurements were prepared by compressing the raw polymers to 2-mm thick sheets under a pressure of 2 MPa at 80 °C. Two cylindrical disks of 6-mm diameter suitable for use with the double sandwich sample holder of the DMA were punched out from the sheets for each measurement. The dynamic mechanical measurements were performed on NR (natural rubber) and BR (polybutadiene) homopolymers, and on SBR, NBR, EPDM and IIR copolymers using a METTLER TOLEDO DMA/SDTA861^e dynamic mechanical analyzer.

Measurements and results

First of all, the complex shear modulus was measured for each sample as a function of temperature.

To do this, the raw polymer was first cooled to well below its glass transition temperature. The complex modulus was then meas-

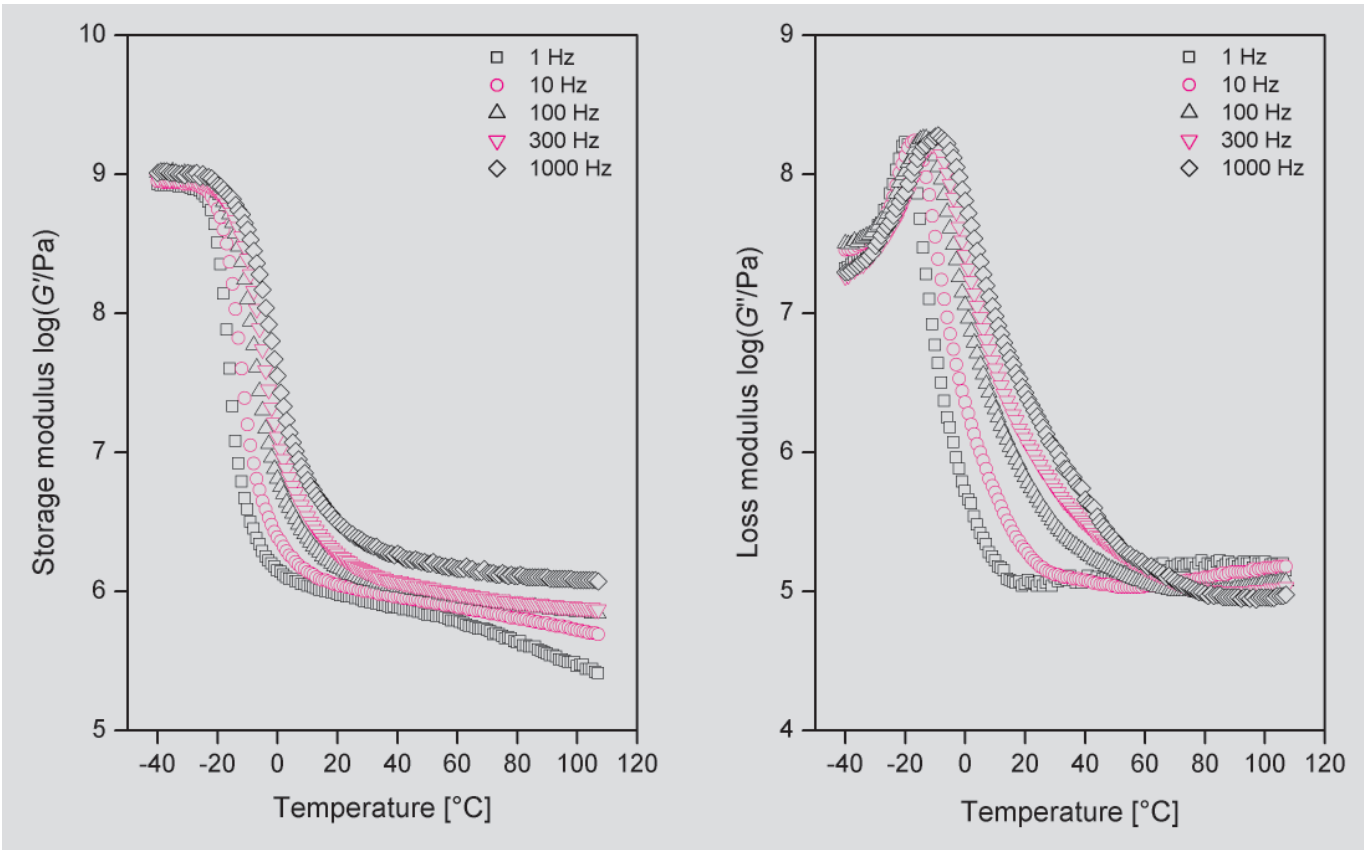

Fig. 1. Temperature-dependent modulus measurements of VSL5025-0 (L-SBR with contents of 25% styrene and 50% vinyl) at different frequencies.

ured at five frequencies (1 Hz, 10 Hz, 100 Hz, 300 Hz and 1000 Hz) at a heating rate of 1K/min up to a temperature of 100 °C. Figure 1 shows the curves obtained from the temperature-dependent measurement of solution-polymerized styrene-butadiene rubber (L-SBR) with contents of 25% styrene and 50% vinyl (polybutadiene in 1,2 position). The glass transition temperatures can be determined from the temperature maxima of the loss moduli. As expected, the glass transition temperature increases with increasing measuring frequency.

The samples that did not exhibit any crystallization effects in the temperature range measured were then cooled again to a temperature below the glass transition temperature (usually about 20 K lower than the glass temperature determined at 1 Hz). Frequency-dependent measurements of the complex shear modulus were then performed at constant temperature at temperature intervals of 10 K. Above 0 °C the temperature interval was increased to 20 K. The final temperature for all measurements was 160 °C.
Master curves were then constructed from the individual measurements over frequency at different temperatures by frequency shifting. The result of master curve construction for L-SBR is displayed in Figure 2 as an example. A reference temperature of -20 °C was chosen for this curve. The small diagram in the upper left part of Figure 2 shows the shift factors, $\log(a_T)$, of the individual frequency-dependent measurements as a function of the measuring temperature.
Relaxation frequency is temperature dependent. The quantitative relationship can be determined by temperature- and frequency-dependent measurements of the shear modulus followed by master curve construction. The reference temperature of the master curve is usually chosen so that the maximum of the loss modulus, G″, is at a frequency of 1 Hz. With temperature-dependent measurements and a measuring frequency of 1 Hz, this reference temperature corresponds approximately to the temperature at which the maximum in the G″ curve appears.

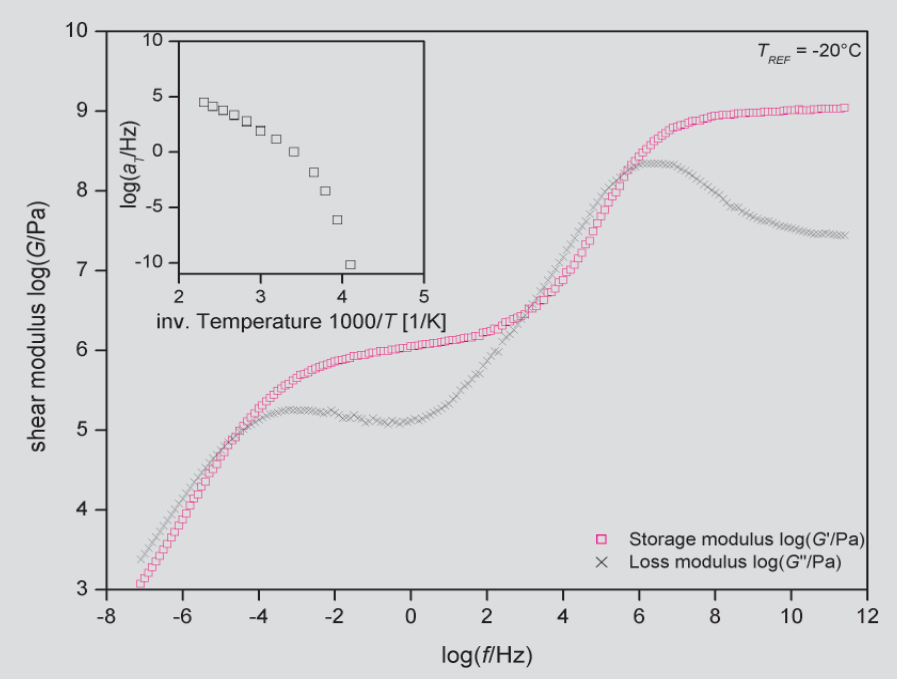

Fig. 2. The master curve of VSL5025-0 constructed from frequency-dependent measurements at a reference temperature of -20 °C, and the shift diagram (upper left).

Figure 3 displays the shift factors of the master curves (open symbols) and the temperature of the maxima of the loss moduli of the temperature-dependent measurements at the five measured frequencies (solid symbols) for all the polymers studied (see Fig. 1). It was not possible to construct a master curve of polybutadiene - the crystallization that occurred due to the high cis 1,4 content and the associated stereo-regularity of the polymer chains influenced the kinetics of the glass relaxation process.
For this reason, only the temperature maxima of the loss moduli from the temperature-dependent modulus measurements were used for evaluation.

Temperature and frequency can be related quantitatively through the semi-empirical WLF equation or the equivalent Vogel-Fulcher equation (see equations 1 and 2).

$$\log(f) = \log(f_R) + \frac{c_1 \cdot (T - T_R)}{c_2 + (T - T_R)} \qquad (1)$$

c_1, c_2 : WLF constants
f_R, T_R : reference frequency or reference temperature

$$f = f_0 \cdot e^{-\frac{\Delta E}{R \cdot (T - T_{VF})}} \qquad (2)$$

f_0 : limiting frequency for $T \rightarrow \infty$
ΔE : activation energy for $T \rightarrow \infty$
T_{VF} : Vogel-Fulcher temperature
R : universal gas constant
(= $8.3144 \cdot 10^{-3}$ kJ/(K·mol))

The formal relationship between the WLF and Vogel-Fulcher equations is given by the equations $c_1 = \frac{\Delta E \cdot \log(e)}{R \cdot (T_R - T_{VF})}$ and $c_2 = (T_R - T_{VF})$.

The continuous lines in Figure 3 correspond to fits of the shift data and the temperature maxima of the loss moduli to the Vogel-Fulcher equation, whereby the parameters f_0, D_E and the temperature, T_{VF}, were used as fit parameters. The parameters of the Vogel-Fulcher equation calculated for each polymer are summarized in Table 1.

The Vogel-Fulcher equation provides a good description of the relationship between frequency and temperature for all the raw polymers studied. The parameter, f_0, is identical within experimental accu-

racy for all the polymers studied. In the dislocation concept, this parameter corresponds to the probability of a dislocation at infinitely high temperature. The parameter, D_E, is comparable for all the polymers studied with the exception of IIR. This parameter characterizes the energy barrier of the dislocation process at temperatures where $T >> T_{VF}$. The Vogel-Fulcher temperature, T_{VF}, is polymer specific and gives the temperature at which the relaxation times of the cooperative relaxations processes taking place in the polymer converge to infinity.

Summary

Both temperature-dependent modulus measurements at different frequencies and frequency-dependent measurements at different temperatures were performed on all the polymers studied . The combination of the two methods allowed the experimental relationship between the temperature and frequency location of the glass process to be determined and quantified by fitting the experimental data to the empirical Vogel-Fulcher equation. With the exception of polyisobutylene (IIR), it was shown that all the samples studied can be described within measurement accuracy by identical Vogel-Fulcher parameters, f_0 and D_E.
The glass transition temperature limits the practical use of elastomeric materials at low temperatures. Since the glass process is also frequency dependent, the behavior of these materials at low temperatures also depends on the frequency of the dynamic stress. The low-temperature behavior can be characterized through a combination of temperature- and frequency-dependent measurements of the shear modulus and a quantitative description on the basis of the time-temperature superposition principle using the empirical Vogel-Fulcher equation.

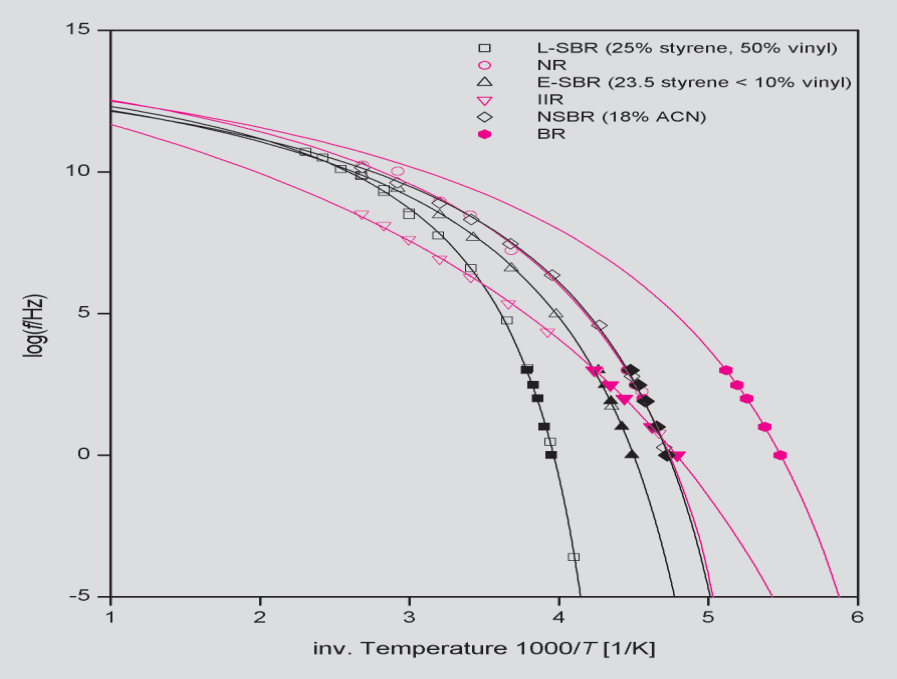

Fig. 3. Shift factors (open symbols) and temperature maxima of the loss factors (solid symbols).

Polymer	ΔE [kJ/mol]	f_0 [Hz]	T_{VF} [°C]
L-SBR (25% styrene, 50% vinyl)	9.8(±0,6)	$9(\pm3)\cdot10^{12}$	-60.5(±2)
NR (>98% cis1,4 polyisoprene)	12(±1,3)	$2(\pm1)\cdot10^{13}$	-109(±4)
E-SBR (23.5% styrene, 12% vinyl)	10.5(±0,8)	$8(\pm3)\cdot10^{12}$	-96(±2)
IIR (double bond content 0.9%)	22.2(±0,2)	$1(\pm0.5)\cdot10^{13}$	-153(±2)
NSBR (18% ACN)	10.4(±0,2)	$6(\pm4)\cdot10^{12}$	-104(±2)
BR (>98% cis1,4)	11.0(±0,4)	$1.6(\pm1)\cdot10^{13}$	-135(±2)

Table 1. Vogel-Fulcher parameters

Investigation of the cold crystallization and melting of amorphous linear polyesters by ADSC

S. Montserrat, F. Roman, P. Colomer, Departament de Màquines i Motors Tèrmics, Universitat Politècnica de Catalunya, Carrer de Colom 11, E-08222-Terrassa, Spanien.

Introduction

Ever since its introduction in the early sixties, differential scanning calorimetry (DSC) has been used as one of the main techniques to study the crystallization and melting of polymers [1].

The cold crystallization and melting of polyethylene terephthalate (PET) was often analyzed with non-isothermal DSC measurements. The degree of crystallinity was then determined from the enthalpies of crystallization and melting by peak area integration [2, 3].

The aim of the present work was to study the crystallization and melting of polyesters using temperature-modulated differential scanning calorimetry (ADSC) and to point out the additional information that can be obtained with this method compared with conventional DSC.

As has already been described elsewhere [4, 5], the ADSC technique is based on the superposition of a sinusoidal temperature program on a linear heating rate program according to the equation

$$T = T_0 + \beta_0 t + A_T \sin(\omega t) \quad (1)$$

where T_0 is the initial temperature, β_0 the underlying (or mean) heating rate, A_T is the temperature amplitude and ω is the modulation frequency. The instantaneous heating rate, β, is given by

$$\beta = \beta_0 + A_T \omega \cos(\omega t) \quad (2)$$

With crystallization and melting measurements, the instantaneous heating rate should always be positive, i.e. $\beta \geq 0$. This is the case when the modulation parameters are chosen so that the condition

$$A_T \leq \frac{\beta_0}{2\pi / p} \quad (3)$$

is satisfied, where p is the modulation period ($p = 2\pi/\omega$). For example, if the underlying heating rate, β_0, is 2 K/min, the condition $\beta \geq 0$ is satisfied for the following pairs of values of A_T and p:
0.159 K and 30 s; 0.318 K and 60 s; and 0.477 K and 90 s.

Modulation of the heating rate of course results in a modulated heat flow curve. Fourier analysis is then used to separate the curve into different components:

i) The total heat flow, ϕ_{tot}, which corresponds to the heat flow that would be obtained with conventional DSC at the same heating rate, β_0.

ii) The phase angle, δ, between the modulated heat flow and the heating rate. This phase shift occurs during the ADSC measurement due to relaxation processes.

iii) A complex heat capacity, $C_p^* = C_p' + iC_p''$, whose modulus is defined by the ratio of the amplitudes of the heat flow, A_ϕ, and the heating rate, A_β, given by

$$|C_p^*| = \frac{A_\phi}{A_\beta} \quad (4)$$

The real and imaginary parts of C_p^* are defined by the equations

$$C_p' = |C_p^*| \cos \delta \quad (5)$$

$$C_p'' = |C_p^*| \sin \delta \quad (6)$$

The real part, C_p', allows the so-called reversing heat flow, ϕ_{rev}, to be calculated through multiplication of C_p' by β_o. In the glass transition region, the phase angle, δ, is very small; cos δ is therefore close to 1 and C_p' is practically equal to $|C_p^*|$.

Experimental details

The samples measured were films of polyethylene terephthalate (PET) and polyethylene 2,6 naphthaline dicarboxylate (PEN). The ADSC analyses were performed using a METTLER TOLEDO DSC821^e equipped with an IntraCooler cooling accessory. The results were evaluated with the STAR^e ADSC software option.

To ensure optimum results, the modulation parameters were chosen so that $\beta \geq 0$ (see equation 3), and all the necessary blank curves and calibration measurements performed. The ADSC curves were measured with $\tau_{lag} = 0$.

Sample weights of 5 to 6 mg and a purge gas flow of 50 ml/min nitrogen were used for all the analyses.

Results and discussion

The heat flow curves of the crystallization and melting of PET

Figure 1 displays the heat flow curves for amorphous PET measured at an underlying heating rate, β_0, of 3 K/min, an amplitude of 0.2 K and a period of 50 s. The total heat flow curve, ϕ_{tot}, shows a glass transition in the range 60 to 90 °C. The glass transition temperature, T_g, is at 76 °C. A relaxation peak due to physical aging of the sample at room temperature is visible slightly below this temperature. There then follows an exothermic peak between 110 and 140 °C corresponding to the cold crystallization of PET, and an endothermic peak between 230 and 270 °C in the region of the melting process.

The enthalpies of crystallization, ΔH_c, and melting, ΔH_s, obtained by integrating the peak areas are -33.3 J/g and +54.6 J/g respectively. The negative value of ΔH corresponds to an exothermic process such as for crystallization, and a positive value to an endothermic process such as for melting. The sum of these two values results in an

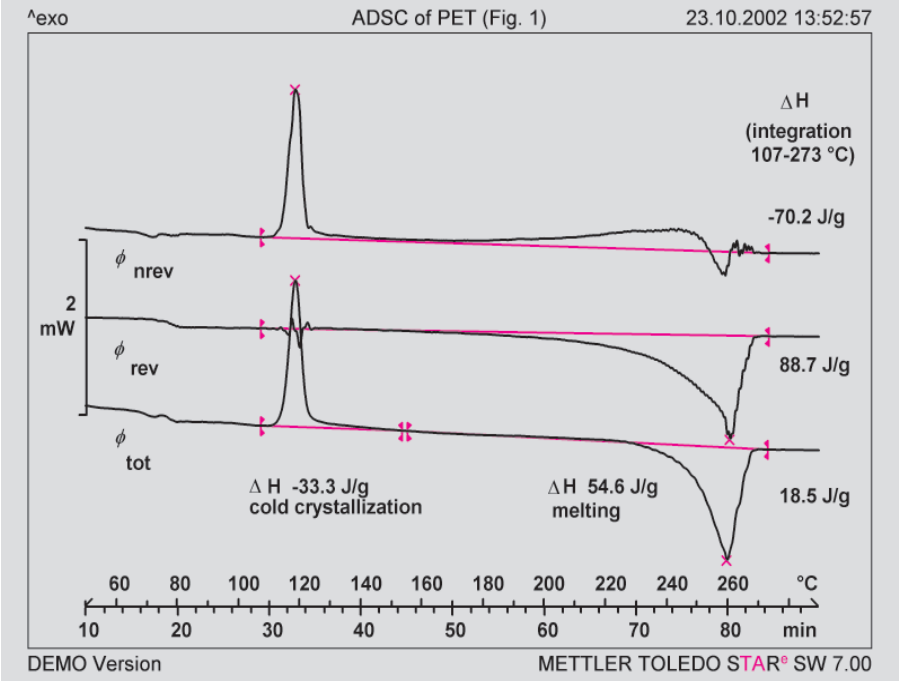

Fig. 1. The total heat flow, ϕ_{tot}, reversing heat flow, ϕ_{rev}, and non-reversing heat flow, ϕ_{nrev}, curves of a PET film obtained from ADSC measurements with an underlying heating rate of 3 K/min, an amplitude of 0.2 K and a period of 50 s. The values of the integrals between the beginning of cold crystallization (107 °C) and the end of melting (273 °C) are shown for the different heat flow curves.

endothermic value of 21.3 J/g, which can be attributed to the melting of the originally crystalline part of the sample.
Some authors [2, 3] recommend calculating the crystallinity by integrating both areas using a baseline drawn from the beginning of cold crystallization through to the end of melting. This procedure yields an endothermic value of +18.5 J/g. Assuming an estimated value of 140 J/g for the enthalpy of melting of 100% crystalline PET, the degree of crystallinity of the sample is then calculated to be 13.2%. The total heat flow gives the same information as that obtained by conventional DSC using a heating rate of 3 K/min.

Figure 1 also displays the so-called reversing heat flow curve, ϕ_{rev}. This shows two thermal events namely the glass transition and the endothermic melting peak.
In contrast to the total heat flow curve, the reversing heat flow curve does not show any effects due to aging in the glass transition region. The glass transition temperatures measured in the ϕ_{tot} and ϕ_{rev} curves are not the same. In the ϕ_{rev} curve, the frequency-dependent dynamic glass transition is measured, whereas the ϕ_{tot} curve displays the thermal glass transition, which is dependent on the heating rate [5 - 7].

The ϕ_{rev} curve is insensitive toward cold crystallization but a small oscillation is nevertheless observed. This is due to the limited number of time periods during the crystallization. It disappears if shorter periods are used (for example a modulation with 2 K/min, 30 s and 0.159 K). Above the glass transition, the ϕ_{rev} curve shows only an endothermic melting peak with an enthalpy change, $\Delta H(\phi_{rev})$, of 88.7 J/g. This is larger than the value calculated from the total heat flow (54.6 J/g). In addition, it can be seen that melting begins at 150 °C, i.e. about 80 K lower than the beginning of melting observed in the ϕ_{tot} curve.

During cold crystallization, metastable crystallites of different size are formed. These continually melt and recrystallize throughout the heating program until melting is finally complete [1]. This continuous melting is detected by the complex heat capacity and shown in the ϕ_{rev} curve. Since melting and recrystallization processes are dependent on heating rate, the enthalpy of melting, $\Delta H_s(\phi_{rev})$, observed in the reversing heat flow curve depends on the modulation conditions. The longer the period, the larger is the observed enthalpy of melting (see Fig. 2).

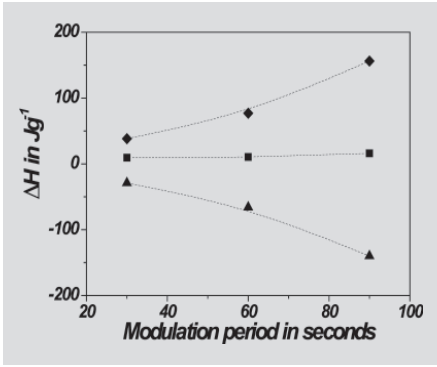

Fig. 2. Effect of the period on the values of ΔH obtained by integration of the total heat flow (■), the reversing heat flow (◆) and the non-reversing heat flow (▲). The underlying heating rate was 2 K/min. The amplitude was chosen so that β 0, i.e. 0.159 K for 30 s, 0.318 K for 60 s, and 0.477 K for 90 s. These results were obtained with a PET film.

The difference between the total heat flow and the reversing heat flow is known as the so-called non-reversing heat flow, ϕ_{nrev}, given by

$$\phi_{nrev} = \phi_{tot} - \phi_{rev} \qquad (7)$$

The ϕ_{nrev} curve is displayed in the upper part of Figure 1 and shows the cold crystallization and the recrystallization process beginning at 150 °C and ending at about 250 °C. Integration of the area under the ϕ_{nrev} curve with the same limits used for the ϕ_{tot} and ϕ_{rev} curves gives an exothermic value of -70.2 J/g for $\Delta H(\phi_{nrev})$. This value, of course, corresponds to the difference between the corresponding enthalpy changes of ϕ_{tot} and ϕ_{rev} according to equation 7, i.e.

$$\Delta H(\phi_{nrev}) = 18.5 - 88.7 = -70.2 \text{ J/g}$$

The non-reversing heat flow curve does not in fact provide any new quantitative information; it does, however, help to visualize the cold crystallization and recrystalliza-

tion processes. On the other hand, the reversing heat flow curve shows the melting process; it should however be noted that this process takes place under non-isothermal conditions and that it is thermodynamically an irreversible process.
The term "reversing heat flow" in fact has nothing to do with "thermodynamically reversible" as is often assumed in connection with temperature-modulated DSC. Both the reversing and the non-reversing heat flows are the result of an irreversible process that occurs under non-equilibrium conditions .

The crystallization and melting region of PEN

In polyesters with several different crystalline forms, ADSC can often improve the separation of peaks and contribute to a better understanding of the crystallization-melting region. This is also the case with PEN. The ADSC heat flow curves of this material are displayed in Figure 3. The total heat flow curve shows a glass transition between 100 and 140 °C (T_g is 117 °C), a cold crystallization between 150 and 190 °C, and melting in the range 250 to 280 °C. In addition, a weak exothermic peak at about 240 °C is observed, which is characteristic for PEN. This peak is attributed to the crystallization of another crystalline form in agreement with other authors [8] .

The reversing heat flow curve shows a melting process that begins practically at the end of the first crystallization peak (190 °C). The main melting peak has a shoulder at about 240 °C due to the (exothermic) crystallization of the second crystalline form.

Both crystallization processes and the recrystallization process can be seen in the non-reversing heat flow curve up to about 265 °C. ADSC clearly shows the presence of two different crystal forms in this thermoplastic material. This effect has previously been studied by DSC and X-ray diffraction techniques [8].

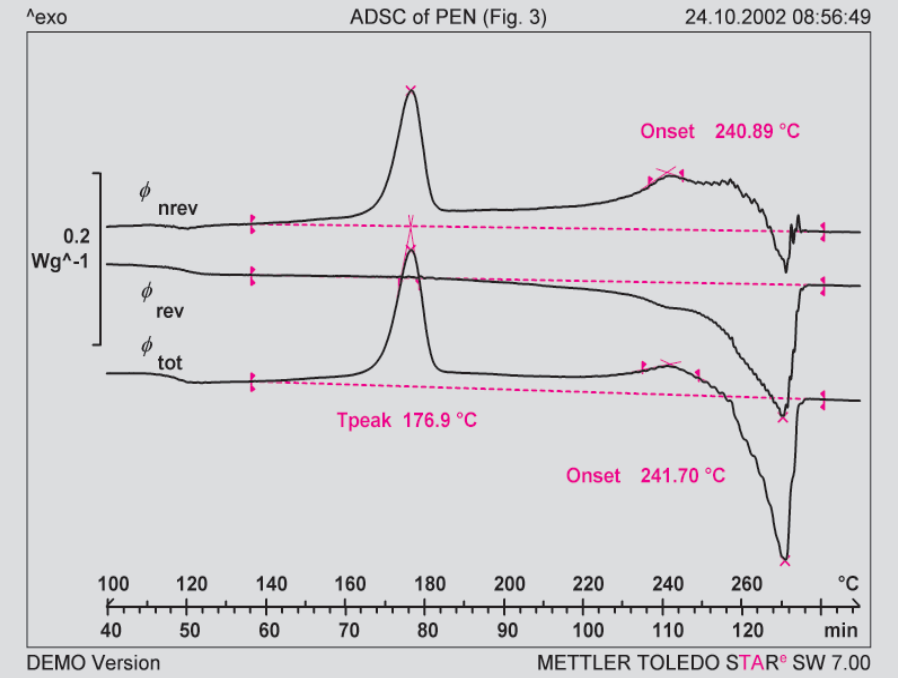

Fig. 3. The total heat flow, ϕ_{tot}, reversing heat flow, ϕ_{rev}, and non-reversing heat flow, ϕ_{nrev}, curves of a PEN film obtained from ADSC measurements with an underlying heating rate of 2 K/min, an amplitude of 0.318 K and a period of 60 s. The temperature maximum of the crystallization peak is given for the total and non-reversing heat flow curves.

Literature

[1] *B. Wunderlich, Thermal Analysis, Academic Press, New York, 1990.*
[2] *K. H. Illers, Colloid Polym Sci 258 (1980) 8.*
[3] *M. Schubnell, UserCom 13 (2001) 12.*
[4] *S. Montserrat, Y. Calventus, P. Colomer, UserCom 11 (2000) 17.*
[5] *S. Montserrat, J. Therm Anal Cal 59 (2000) 289.*
[6] *UserCom 11 (2000) 1 and 8.*
[7] *J.E.K. Schawe, Colloid Polym Sci 276 (1998) 565.*
[8] *S. Buchner, D. Wiswe, H.G. Zachman, Polymer 30 (1989) 480.*

Drying and glass transition using IsoStep™

Dr. Jürgen Schawe, Dr. Uwe Hess

Introduction

If several thermal events occur simultaneously in a DSC measurement, the problem is then how to separate the different processes involved. Often, a change in heat capacity is overlapped by exothermic or endothermic peaks, e.g. through chemical reactions, crystallization or vaporization. One possible way to separate the different processes is to vary the measurement conditions in the conventional DSC. For example, heating and cooling measurements can be performed at different rates and in different temperature ranges using different types of crucible. This is of course relatively time-consuming.

IsoStep™ is a new technique that can be used to distinguish between such overlapping processes. It provides both the heat capacity curve and the non-reversing curve simultaneously.

In this article, the separation of different thermal events is demonstrated by measuring the glass transition of a spray-dried pharmaceutical substance. The measurement of a similar compound to determine the change of heat capacity during the vaporization of water has been described in a previous article [1, 2]. As an extension of this, the relationship between the water content and the glass transition temperature is analyzed quantitatively using IsoStep™. Knowledge of this relationship is important for processing the powder because it can become sticky if the glass transition temperature is below the processing temperature.

Experimental details

The DSC measurements were performed with a DSC822^e equipped with an IntraCooler. The STAR^e software with the IsoStep™ option was used for the evaluation.

In the IsoStep™ method, a conventional heat capacity measurement is combined with a quasi-isothermal kinetic evaluation. The temperature program consists of a series of isothermal segments and heating steps. The parameters (length of the isothermal segments, heating rate and step height in the heating step) are not restricted in any way. They can even be different during a measurement depending on the actual task or thermal event investigated. The heat capacity as a function of temperature is obtained from the heat flow during the heating step, and the non-reversing curve from the heat flow during the isothermal step [3]. The measurements described here used temperature steps of 1 K at 2 K/min. The isothermal period at the beginning of the measurement was 30 s. The measuring cell was purged with nitrogen.

The sample used was a spray-dried pharmaceutical product consisting of two amorphous components. The water content of the starting material was analyzed by TGA/SDTA851^e and found to be 6.08%. Samples of about 8 mg were sealed in 40-µl aluminum crucibles with a 50-µm hole in the lid (ME-51140832). The samples were dried each time in the DSC at 80 °C for different periods of time before measurement in order to obtain different water contents. The advantage of this procedure was that the sample did not have to be transported after drying. The small hole in the lid restricts the evaporation of the water so that drying proceeds in a defined way. The moisture content before the beginning the measurement, w_{ini}, was determined by measuring the decrease of the water content during the storage of the crucibles with the TGA/SDTA851^e [4]. Trial experiments in the DSC and TGA showed that the samples did not change chemically during the predrying step.

Results and interpretation

Figure 1 shows a typical IsoStep™ measurement curve as a function of the temperature. The upper limit of the curve corresponds to the heat flow during the isothermal segments, from which the non-reversing curve is calculated.

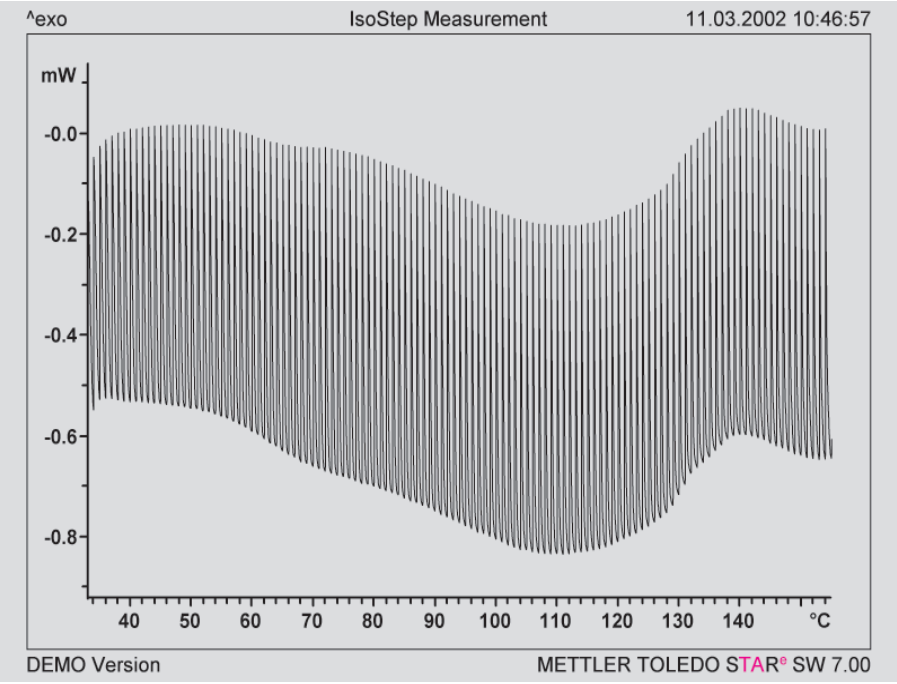

Fig. 1. IsoStep™ measurement as a function of the temperature of a sample that had been preheated at 80 °C for 20 min.

Figure 2 shows the heat capacity and the non-reversing curves of the material that had been heated beforehand for 20 minutes. In the heat capacity curve, two glass transitions can be seen at about 70 °C and 125 °C. The broad vaporization peak observed in the non-reversing curve overlaps both glass transitions. This peak is so large that the glass transitions are not resolved in a conventional DSC curve. The first glass transition depends on the water content and is responsible for the powder sticking. Its glass transition temperature, T_g, was therefore investigated as a function of water content.
In the heat capacity curves (Fig. 3), one can see the shift of the glass transition temperature to higher temperature after longer drying times.

The water content before the measurement, w_{ini}, is of course not the same as the water content at the glass transition temperature, w_{Tg}, because water escapes continuously from the sample during the measurement.
This loss of water can be determined from the non-reversing curve by evaluating the partial peak area up to T_g. The relevant partial peak area, Δh_p, is shown by the hatched area in Figure 2.

If the specific heat of vaporization of water, Δh_w, is known, the water content up to T_g can be determined from the equation

$$w_{Tg} = w_{ini} - \frac{\Delta h_p}{\Delta h_w} \cdot 100\% \qquad (1)$$

Δh_w can be determined from the total peak area on vaporization, ΔH, and the loss of mass during the measurement, Δm, (determined by re-weighing): $\Delta h_w = \Delta H/\Delta m$ [4]. A value of 2500 J/g was obtained for Δh_w [2]. This is somewhat greater than the value for free water (2400 J/g).

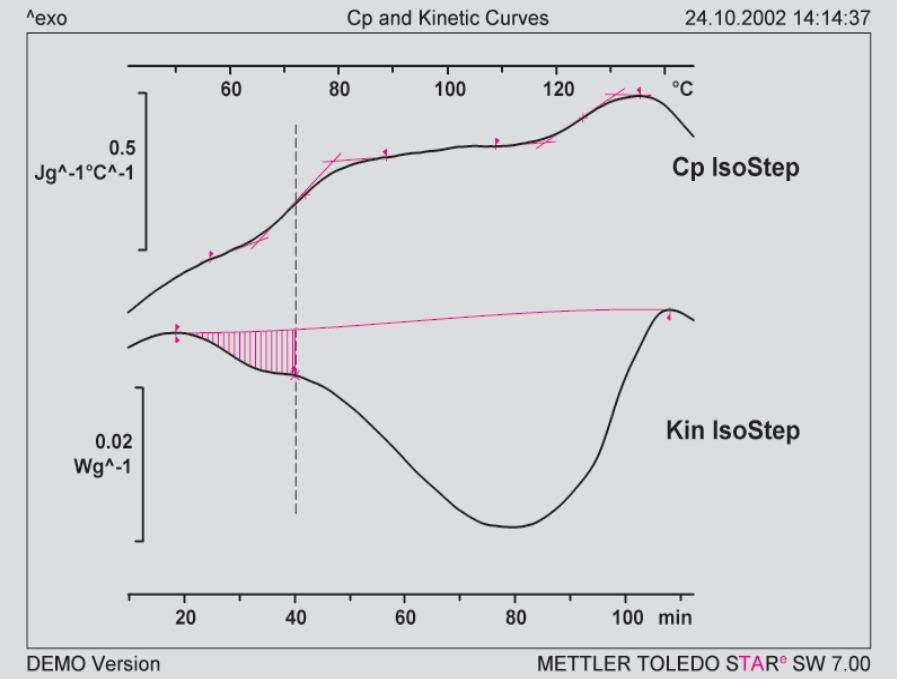

Fig. 2. Specific heat capacity and non-reversing (kinetic) curves as a function of the temperature or measurement time, calculated from the measurement in Figure 1. The hatched area shows the amount of water vaporized up to the glass transition temperature.

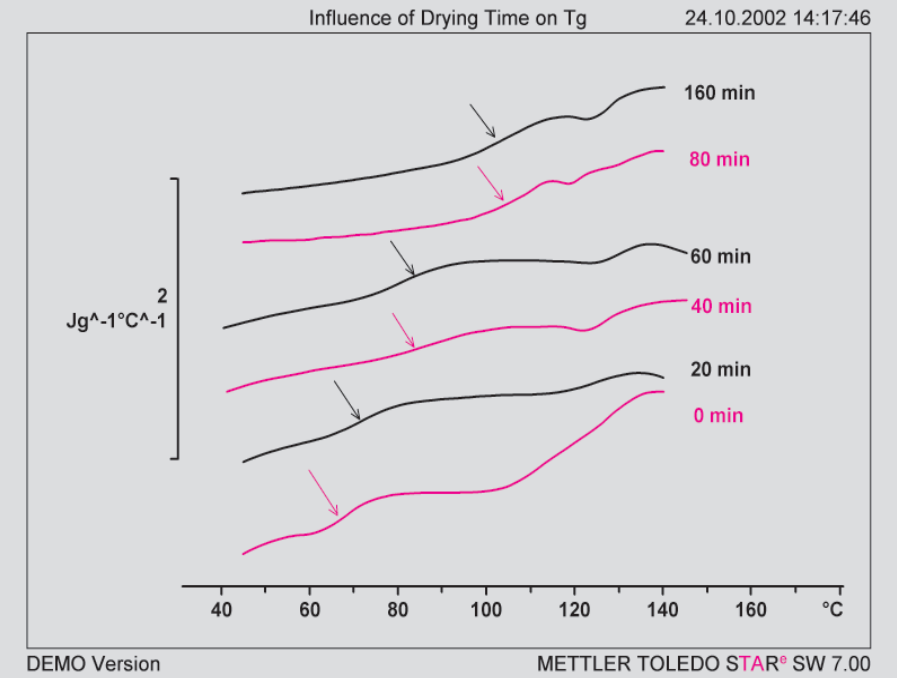

Fig. 3. Heat capacity curves measured after different drying times at 80 °C. The parameter is the drying time. The arrows point to the glass transition temperatures.

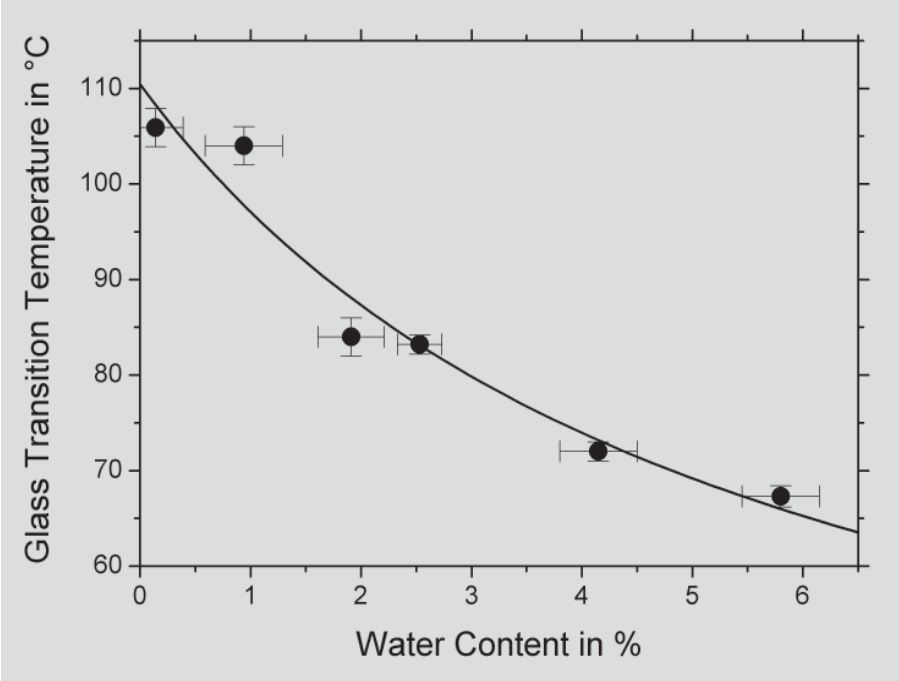

Fig. 4. Glass transition temperature as a function of water content at T_g.

The glass transition temperatures determined from the curves in Figure 3 are displayed in Figure 4 as a function of the water content, w_{Tg} (Eq. (1)). This diagram can be used to optimize the processing conditions for the material.

Summary

With IsoStep™, the heat capacity and the non-reversing curve can be determined simultaneously in one measurement. This allows glass transition and vaporization processes to be separated.

With a spray-dried pharmaceutical substance, it has been shown that the method can be used to quantitatively determine the effect of moisture on the glass transition temperature. The measurement procedure features easy sample preparation, direct measurement and high accuracy.

Literature

[1] *M. Schubnell, J. Schawe, UserCom 14 (2001) 5.*

[2] *M. Schubnell, J.E.K. Schawe, Int. J. Pharm., 192 (2001) 173.*

[3] *U. Joerimann, UserCom 15 (2002).*

[4] *J.E.K. Schawe, U. Hess, J. Thermal Anal. Cal., 68 / 2002 / 741.*

Dates

Exhibitions, Conferences and Seminars - Veranstaltungen, Konferenzen und Seminare

SIAT 2003, Symposium on International Automotive Technology in association with SAE International	January 15-18, 2003	ARAI, Pune (India)
15. Ulm-Freiberger Kalorimetrietage	19. bis 21. März 2003	Freiberg, Sachsen (Deutschland)
INSTRURAMA	April 2-4, 2003	Brussels (Belgium)
TAC	April 15-16, 2003	Huddersfield (UK)
PLAST	06-10, Maggio 2003	Milano (Italy)
AFCAT (Association de Calorimétrie et d'Analyse Thermique)	May, 2003	Mulhouse (France)
PhandTA 7		
Int. Conference / Workshop on Pharmacy and Applied Physical Chemistry	7. bis 11. September, 2003	Innsbruck (Oesterreich)
NATAS 2003	September 22-24, 2003	Albuquerque (USA)
Het Instrument 2002	4-8 Novembre, 2003	Utrecht (Netherlands)
RICH MAC	25-28 Novembre, 2003	Milano (Italy)

TA Customer Courses and Seminars in Switzerland - Information and Course Registration:
TA-Kundenkurse und Seminare in der Schweiz - Auskunft und Anmeldung bei:

Frau Esther Andreato, METTLER TOLEDO GmbH, Schwerzenbach, Tel: ++41 1 806 73 57, Fax: ++41 1 806 72 40, e-mail: esther.andreato@mt.com

Courses/Kurse:

TMA-DMA/SW Basic (Deutsch)	17. Februar 2003	TMA-DMA/SW Basic (English)	February 24, 2003
TGA (Deutsch)	18. Februar 2003	TGA (English)	February 25, 2003
DSC Basic (Deutsch)	19. Februar 2003	DSC Basic (English)	February 26, 2003
DSC Advanced (Deutsch)	20. Februar 2003	DSC Advanced (English)	February 27, 2003
SW Advanced (Deutsch)	21. Februar 2003	SW Advanced (English)	February 28, 2003
TMA-DMA/SW Basic (Deutsch)	22. September 2003	TMA-DMA/SW Basic (English)	September 29, 2003
TGA (Deutsch)	23. September 2003	TGA (English)	September 30, 2003
DSC Basic (Deutsch)	24. September 2003	DSC Basic (English)	October 01, 2003
DSC Advanced (Deutsch)	25. September 2003	DSC Advanced (English)	October 02, 2003
SW Advanced (Deutsch)	26. September 2003	SW Advanced (English)	October 03, 2003

TA-Kundenkurse und Seminare (Deutschland)

Für nähere Informationen wenden Sie sich bitte an: Frau Ina Wolf, METTLER TOLEDO GmbH, Giessen, Tel: ++49 641 507 404

Cours et séminaires d'Analyse Thermique en France

Renseignements et inscriptions par Christine Fauvarque, METTLER TOLEDO S.A., Viroflay, Tél: ++33 1 3097 1439, Fax: ++33 1 3097 1660

Cours clients :

TG et logiciel STARe	14 avril 2003 Viroflay (France)	TG et logiciel STARe	07 octobre 2003 Viroflay (France)
DSC et logiciel STARe	15 avril 2003 Viroflay (France)	DSC et logiciel STARe	08 octobre 2003 Viroflay (France)
DSC avancé et logiciel STARe	16 avril 2003 Viroflay (France)	DSC avancé et logiciel STARe	09 octobre 2003 Viroflay (France)
		DMA/TMA et logiciel STARe	10 octobre 2003 Viroflay (France)
Utilisation de l'analyse thermique dans le domaine de la sécurité des procédés (Institut de Sécurité de Bâle)			17 avril 2003 Viroflay (France)
DMA/TMA et logiciel STARe	18 avril 2003 Viroflay (France)		

Seminars for Thermal Analysis in Belgium

Registration: Pat Hoogeras, N.V. METTLER TOLEDO S.A., Zaventem, Tél: ++32 2 334 02 09, Fax: ++32 2 334 03 34
The dates are not yet definite; please check.

Seminar on high-throughput methods for Thermal Analysis. Which method for which application?	May 15, 2003
Infoday on Thermal Analysis: Principles & Applications	April 30, 2003

TA Customer Courses and Seminars in the Netherlands

We zijn voornemens om in het voorjaar 2003, Maart of April wederom enkele seminars te organiseren.
Voor verdere informatie kunt U kontakt opnemen met: Hay Berden of Ko Schaap, Mettler-Toledo B.V., Tiel, Tel: ++31 344 63 83 63

Corsi e Seminari di Analisi Termica per Clienti in Italia

Per ulteriori informazioni prego contattare:
Simona Ferrari, Mettler-Toledo S.p.A., Novate Milanese, Tel: ++39 02 333 321, Fax: ++39 02 356 2973, E-mail: simona.ferrari@mt.com

Corsi per Clienti:

DSC base	4 Marzo 2003,	3 Giugno 2003,	16 Settembre 2003	Novate Milanese
DSC avanzato	5 Marzo 2003,	4 Giugno 2003,	17 Settembre 2003	Novate Milanese
TGA	6 Marzo 2003,	5 Giugno 2003,	18 Settembre 2003	Novate Milanese
TMA	7 Marzo 2003,	6 Giugno 2003,	19 Settembre 2003	Novate Milanese

InfoDays / Workshops:

Caratterizzazione dei materiali polimerici.
L'impiego dell'analisi termica DSC, TGA, TMA, DMA e di metodi chimici per l'analisi dell'umidità.
Aspetti teorici, scelta dei metodi, interpretazione dei risultati, esempi applicativi.

Milano	21 Gennaio 2003	Bologna	27 Febbraio 2003	Torino	15 Maggio 2003
Roma	11 Febbraio 2003	Firenze	12 Marzo 2003		

Cursos y Seminarios de TA en España

Para detalles acerca de los cursos y seminarios, por favor, contacte con:
Francesc Catala, Mettler-Toledo S.A.E., Tel: ++34 93 223 76 00, E-Mail: francesc.catala@mt.com

Seminario de aplicaciones TA:	Julio 2, 2003 Madrid	Seminario de aplicaciones TA:	Julio 09, 2003 Barcelona
Seminario para usuarios STARe:	Julio 3, 2003 Madrid	Seminario para usuarios STARe:	Julio 10, 2003 Barcelona
VIII Reunión del GEP	Septiembre 14-17, 2003 Tarragona		

TA Customer Courses and Seminars for Sweden and the Nordic countries

For details of training courses and seminars, please contact:
Fredrik Einarsson, Mettler-Toledo AB, Tel: ++46 455 30 0080, Fax: ++46 8 642 45 62, E-mail: fredrik.einarsson@mt.com

Open TA Forum	March 25-26, 2003	Stockholm

TA Customer Courses and Seminars in the UK

For details of training courses and seminars, please contact:
Rod Bottom, METTLER TOLEDO Ltd Leicester, Tel: ++44 116 234 5025, Fax: ++44 116 236 5500

TA Customer Courses and Seminars in the USA and Canada

Basic Thermal Analysis Training based on the STARe System Versions 6 and 7 is being offered in California and at the Columbus, Ohio Headquarters. The training includes lectures and hands-on workshops.
For information, please contact: Tom Basalik at +1 614 438 4687, Fax: +1 614 438 4693 or by e-mail: mailto:tom.basalik@mt.com

TA Customer Courses in the South East Asia Regional Office, Kuala Lumpur

For information on dates, please contact:
Malaysia: Ricky Tan at ++603 78455773, Fax: 603 78458773
Singapore: Joselyn Yeo at ++65 8900011, Fax: 65 8900013
Thailand: W. Techakasembundit at ++662 7230336, Fax: 662 7196479
or SEA regional office: Soosay P. at ++603 78455373, Fax: 603 78453478

TA Customer Courses and Seminars in Japan

For details of training courses and seminars, please contact:
Yasushi Ikeda at METTLER TOLEDO Japan, Tel: ++81 3 5762 0746, Fax: ++81 3 5762 0758, or by e-mail: yasushi.ikeda@mt.com

TA Customer Training	March 11-14, 2003	Tokyo & Osaka Service Center
TA Customer Training	August 26-29, 2003	Tokyo & Osaka Service Center
Infoday Seminar	October 21, 2003	Tokyo Technical Center
Infoday Seminar	October 24, 2003	Osaka Branch

Cursos y Seminarios de TA en Latin America

Para detalles acerca de los cursos y seminarios, por favor, contacte con:
Carlos Alberto Maciel, Mettler-Toledo, Inc, LA, Tel: ++55 11 4166-7400 (Brasil), E-Mail: CarlosAlberto.Maciel@mt.com

Infoday / Seminar Polymers	28 April to 2 May, 2003	São Paulo and Rio de Janeiro - Brazil
Seminario de Aplications TA	06-10 May, 2003	Santiago de Chile - Chile
Exhibition: ANALÍTICA 2003	01-03 Oct, 2003	São Paulo - Brazil
Seminario de Aplications TA	13-17 Oct, 2003	Rio de Janeiro - Brazil
Infoday / Seminar Pharma	21-25 Oct, 2003	Bogotá - Colombia

TA Seminars in Taiwan

For details of seminars, please contact:
Kimmy Wu at METTLER TOLEDO Taiwan, Tel: ++886 2 25795955, Fax: ++886 2 25795977

For further information regarding meetings, products or applications, please contact your local METTLER TOLEDO representative.
Bei Fragen zu weiteren Tagungen, den Produkten oder Applikationen wenden Sie sich bitte an Ihre lokale METTLER TOLEDO Vertretung.
Internet: http:/www.mt.com

Editorial team


Dr. J. Schawe, Physicist


Dr. R. Riesen, Chem. Engineer


J. Widmann, Chem. Engineer


Dr. M. Schubnell, Physicist


C. Darribère, Chem. Engineer


Dr. M. Wagner, Chem. Engineer


Dr. D. P. May Chemist


Ni Jing Chemist


Urs Jörimann Electr. Engineer

METTLER TOLEDO GmbH, Analytical, Sonnenbergstrasse 74, CH-8603 Schwerzenbach, Switzerland
Contact: urs.joerimann@mt.com, Tel: ++41 1 806 73 87, Fax: ++41 1 806 72 60
Internet: http:/www.mt.com/ta

ME-51724323

Printed on 100% chlorine-free paper, for the sake of the environment.

METTLER TOLEDO